

# Dynamic Response Functions from Angle Resolved Photoemission Spectra

U. Chatterjee,<sup>1,2</sup> D. K. Morr,<sup>1</sup> M. R. Norman,<sup>2</sup> M. Randeria,<sup>3</sup> A. Kanigel,<sup>1</sup> M. Shi,<sup>1,4</sup> E. Rossi,<sup>1</sup> A. Kaminski,<sup>5</sup> H. M. Fretwell,<sup>5</sup> S. Rosenkranz,<sup>2</sup> K. Kadowaki,<sup>6</sup> and J. C. Campuzano<sup>1,2</sup>

<sup>1</sup>*Department of Physics, University of Illinois at Chicago, Chicago, IL 60607*

<sup>2</sup>*Materials Science Division, Argonne National Laboratory, Argonne, IL 60439*

<sup>3</sup>*Department of Physics, The Ohio State University, Columbus, OH 43210*

<sup>4</sup>*Swiss Light Source, Paul Scherrer Institut, CH-5232 Villigen, Switzerland*

<sup>5</sup>*Ames Laboratory and Department of Physics and Astronomy, Iowa State University, Ames, IA 50011*

<sup>6</sup>*Institute of Materials Science, University of Tsukuba, Ibaraki 305-3573, Japan*

(Dated: December 27, 2021)

We introduce a formalism for calculating dynamic response functions using experimental single-particle Green's functions. As an illustration of this procedure we estimate the dynamic spin response of the cuprate superconductor  $\text{Bi}_2\text{Sr}_2\text{CaCu}_2\text{O}_{8+\delta}$ . We find good agreement with superconducting state neutron data, in particular the  $(\pi, \pi)$  resonance with its unusual 'hourglass' shaped dispersion. We anticipate our formalism will also be useful in interpreting results from other spectroscopies, such as optical and Raman responses.

PACS numbers: 74.25.Jb, 74.25.Ha, 74.72.Hs, 79.60.Bm

The linear response to an external probe as a function of momentum and frequency is of great importance in elucidating the properties of complex materials. Examples include various two-particle correlation functions involving spin, current and charge as measured by inelastic neutron scattering (INS), nuclear magnetic resonance (NMR), optical conductivity, and Raman scattering experiments. On the other hand, angle resolved photoemission spectroscopy (ARPES) [1] directly gives information about single-particle excitations of a system. The response function of a system can be expressed in terms of a two-particle correlation function of the observable to which the external probe couples. The goal of this paper is to develop an approach to use single-particle spectroscopy data to gain insight into two-particle correlation functions. In particular we focus here on using the Green's functions obtained from superconducting state ARPES data in the high  $T_c$  cuprates to compute the dynamic spin susceptibility, which we then compare with INS data [2].

From a theoretical point of view, dynamic response functions are difficult to calculate in general and many different approximate formalisms exist in the literature. For instance, there are two rather different approaches for computing the dynamic spin response for the high  $T_c$  cuprate superconductors. The first is based on the random phase approximation (RPA) [3] and related diagrammatic formulations [4]. This approach not only assumes momentum is a good quantum number, but also that the spin and charge degrees of freedom are coupled. The second is based on spin ladders separated by one-dimensional domain walls known as stripes. In this formalism spatial inhomogeneity is important, and the

charge sector is assumed to be secondary when calculating the spin response [5]. Despite the quite different physics underlying these two schemes, the results for the calculated spin response function of the cuprates are similar - one of the current dilemmas facing the field of high  $T_c$  superconductivity. It is thus important to go beyond a purely theoretical approach and directly employ information obtained from one experiment (ARPES) to make progress on interpreting the dynamic susceptibility measured by another (INS).

We use a formalism based on a diagrammatic  $\mathbf{k}$ -space approach which goes beyond RPA in that it uses fully dressed Green's function obtained from ARPES data on  $\text{Bi}_2\text{Sr}_2\text{CaCu}_2\text{O}_{8+\delta}$  (Bi2212). We compare the calculated superconducting state susceptibility with INS data. We obtain the  $(\pi, \pi)$  resonance seen in many cuprates [2], including Bi2212 [6], and also its unusual 'hourglass' shaped dispersion as observed in  $\text{YBa}_2\text{Cu}_3\text{O}_{7-\delta}$  (YBCO) [7, 8] and more recently in Bi2212 [9]. We also find that the magnetic dispersion is sensitive to the momentum dependence of the effective interaction used to calculate the susceptibility.

We use ARPES spectra from a near-optimal sample ( $T_c=90\text{K}$ ) of Bi2212, the data having been presented previously [10, 11]. While a resonance peak was observed in this material some time ago [6], a more detailed study with results similar to the much more extensive INS data for YBCO, has appeared only recently [9].

Quite generally, two-particle correlation functions can be written in terms of single-particle Green's functions and vertex parts [12]. The lowest order term contributing to the spin susceptibility (the bare polarization bubble) in the superconducting state can be written as [13]

$$\chi_0(\mathbf{q}, \Omega) = \frac{1}{\pi^2} \sum_{\mathbf{k}} \int_{-\infty}^{\infty} d\nu d\epsilon [\text{Im}G(\mathbf{k}, \nu) \text{Im}G(\mathbf{k} + \mathbf{q}, \epsilon) + \text{Im}F(\mathbf{k}, \nu) \text{Im}F(\mathbf{k} + \mathbf{q}, \epsilon)] \frac{n_F(\nu) - n_F(\epsilon)}{\Omega + \nu - \epsilon + i\delta} = \chi_0^G + \chi_0^F \quad (1)$$

where  $\text{Im}$  denotes the imaginary part of the normal and anomalous Green's functions  $G$  and  $F$ , and  $\chi_0^G$  and  $\chi_0^F$  denote the  $GG$  and  $FF$  contributions to  $\chi_0$  respectively.

We next describe in detail how  $\text{Im}G$  is extracted from ARPES data and return later to the question of estimating the contribution of  $\text{Im}F$  (which is not directly measured). ARPES probes the occupied part of the spectral function leading to the intensity  $I(\mathbf{k}, \omega) \propto n_F(\omega) \text{Im}G(\mathbf{k}, \omega)$ , where  $n_F(\omega)$  is the Fermi function [14]. In order to extract  $\text{Im}G$  from raw data we need to address several issues including data normalization, background subtraction, and removing the effects of the Fermi function. In addition we need to extend  $\text{Im}G$  to  $\omega > 0$  to calculate  $\chi_0$ .

Starting from raw data, we first subtract the constant signal at  $\omega > 0$  (due to second order light). Next an ‘unoccupied’ state spectrum at a  $k$  far from  $k_F$  is used as an energy-dependent background [15]. The subtraction is performed by normalizing the background to each spectra at a given binding energy,  $\omega_c$  (320 meV for the data set in question), and then subtracting it [16]. This effective spectral function represents the the renormalized band near the Fermi energy. Finally, we divide the data by a resolution [17] broadened Fermi function to obtain  $\text{Im}G(\mathbf{k}, \omega)$  for  $\omega < 0$ .

The next step is to determine the unoccupied part of the spectral function,  $\text{Im}G(\mathbf{k}, \omega)$  for  $\omega > 0$ , which cannot be obtained directly from ARPES data. We obtain this by invoking particle-hole symmetry with respect to the Fermi surface:  $\mathbf{k}_F$ ,  $\text{Im}G(\mathbf{k}_F + \mathbf{k}, \omega) = \text{Im}G(\mathbf{k}_F - \mathbf{k}, -\omega)$ , where  $\mathbf{k}$  is directed along the normal to the Fermi surface. This assumption should be reasonable in the superconducting state of optimally doped cuprates over an energy range in excess of the gap, as evidenced by the approximate particle-hole symmetry seen in tunneling experiments [18]. We have also checked that this assumption does not qualitatively affect our final results for  $\chi_0$  (by using  $\text{Im}G$  with p-h asymmetry put in by hand). We then normalize the obtained  $\text{Im}G$  so that the integral of the spectral function ( $-\text{Im}G/\pi$ ) is equal to unity over the energy range of  $\pm\omega_c$ . This minimizes the effect of dipole matrix elements. Now we may use the  $\text{Im}G$  derived from ARPES to calculate  $\chi_0^G$  (we will discuss  $\chi_0^F$  later). Finally, to perform the  $\mathbf{k}$ -sum in Eq. (1), the ARPES data are interpolated to a regular grid and then reflected using square lattice group operations to fill the first Brillouin zone [11]. We used a  $100 \times 100$  grid.

Fig. 1a shows the calculated  $\text{Im}\chi_0^G$  at  $T=40\text{K}$  (superconducting state) as a function of the momentum transfer

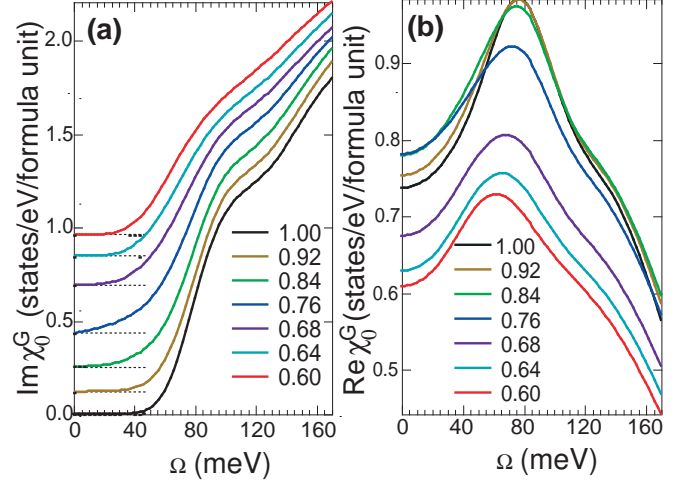


FIG. 1: (a)  $\text{Im}\chi_0^G$  and (b)  $\text{Re}\chi_0^G$  in the superconducting state as a function of frequency for momenta along  $\mathbf{q} = \eta(\pi, \pi)$ . The various curves, labeled by  $\eta$ , are offset for clarity in panel (a), noting that  $\text{Im}\chi_0^G = 0$  at  $\Omega = 0$ .

$\mathbf{q}$  along the zone diagonal. We note that  $\text{Im}\chi_0^G$  is greatly suppressed at low energies due to the gap to particle-hole (p-h) excitations in the superconducting state and then increases quite sharply. The p-h gap is in general given by the sum of the superconducting gaps at two points on the Fermi surface separated by the wavevector  $\mathbf{q}$ . The  $\mathbf{Q} = (\pi, \pi)$  vector connects the hot spots ( $\epsilon_{\mathbf{k}} = \epsilon_{\mathbf{k}+\mathbf{Q}}=0$ ) which are not too far from the zone boundary in Bi2212, and thus the hot-spot gap is comparable to the one at the antinode. Consequentially at  $\mathbf{Q} = (\pi, \pi)$ , we see in Fig. 1a a large gap whose midpoint is around 80 meV, roughly twice the maximum d-wave superconducting gap of  $\simeq 40$  meV at the antinode. We note that the threshold is quite broad ( $\sim 40$  meV) as a result of the intrinsic broadening of  $\text{Im}G$  arising from self-energy effects as well as resolution. As  $q$  decreases from  $Q$ , one sees the p-h gap decrease due to the d-wave anisotropy of the gap, and then disappear at  $\mathbf{q}_n \simeq (0.76, 0.76)\pi$ .  $\mathbf{q}_n$  is the wavevector corresponding to node-node scattering with the d-wave gap vanishing at the nodes. For  $q < q_n$ , the p-h gap reappears [3].

In Fig. 1b we show  $\text{Re}\chi_0^G$  obtained from Eq. (1) [19]. First concentrating on  $\mathbf{Q}$ , we note the presence of a peak that corresponds to the gap midpoint of Fig. 1a as expected from Kramers-Kronig relations. This peak is broadest for  $\mathbf{q}_n$  where the p-h gap vanishes in the imaginary part.

We now turn to  $\chi_0^F$ . Since  $\text{Im}F$  is not available from

experiment, we estimate the FF term as follows. We calculate the BCS  $\chi_{0,\text{BCS}}^G$  and  $\chi_{0,\text{BCS}}^F$  from Eq. (1) using the bare BCS Green's functions  $G_0(\mathbf{k}, \omega) = (\omega + \epsilon_{\mathbf{k}})/(\omega^2 - \epsilon_{\mathbf{k}}^2 - \Delta_{\mathbf{k}}^2)$  and  $F_0(\mathbf{k}, \omega) = \Delta_{\mathbf{k}}/(\omega^2 - \epsilon_{\mathbf{k}}^2 - \Delta_{\mathbf{k}}^2)$  with the experimentally measured dispersion [20]  $\epsilon_{\mathbf{k}}$  and the measured  $\Delta_{\mathbf{k}}$ , which we find to be proportional to  $(\cos k_x - \cos k_y)$  for this sample. We define the ratio of the real and imaginary parts, given by  $\alpha_R(\mathbf{q}, \Omega) = \text{Re}\chi_{0,\text{BCS}}^F/\text{Re}\chi_{0,\text{BCS}}^G$  and similarly for  $\alpha_I(\mathbf{q}, \Omega)$ . We then assume that the missing contribution  $\chi_0^F$  may be accounted for by  $\text{Re}\chi_0 = \text{Re}\chi_0^G + \text{Re}\chi_0^F \simeq (1 + \alpha_R)\text{Re}\chi_0^G$  and  $\text{Im}\chi_0 = \text{Im}\chi_0^G + \text{Im}\chi_0^F \simeq (1 + \alpha_I)\text{Im}\chi_0^G$ . We will discuss below the extent to which our final results are affected by this approximation.

In order to carry out comparisons with INS data, or other probes such as NMR, the full spin susceptibility  $\chi$  is needed. The most common approximation is to use the RPA form [3]

$$\chi(\mathbf{q}, \Omega) = \frac{\chi_0(\mathbf{q}, \Omega)}{1 - U(\mathbf{q})\chi_0(\mathbf{q}, \Omega)} \quad (2)$$

where  $U$  is an effective interaction. In this paper, we will assume two limiting forms for this effective interaction, one where it is a constant ( $U_0$ ), the other where it has the form  $U(\mathbf{q}) = -U_0(\cos q_x + \cos q_y)/2$  corresponding to superexchange between near neighbor copper sites.

The experimental results for  $\chi_0$  presented in Fig. 1 are similar to those obtained from BCS theory [3] especially at low energies where the incoherent spectral weight in the ARPES data is small. Within BCS theory, which uses *bare* Green's functions, one has a true gap in  $\text{Im}\chi_0$  at  $\mathbf{Q}$  and a corresponding log divergence in  $\text{Re}\chi_0$ . These features still persist in Fig. 1 albeit broadened by self-energy (and resolution) effects. As such, for some frequency smaller than the gap, one will obtain a pole in  $\chi$  when  $1 - U(\mathbf{q})\text{Re}\chi_0(\mathbf{q}, \Omega) = 0$  provided  $\text{Im}\chi_0$  is small at the frequency of interest. This pole represents a collective mode, known as the spin resonance at  $\mathbf{Q}$ , which is prominently observed in INS data for YBCO [2] and Bi2212 [6, 9]. Following this logic, we fix  $U_0$  [21] by fitting the energy (44 meV) of the INS spin resonance at  $\mathbf{Q}$  for optimal doped Bi2212 [6].

In order to compare the results of our approach with INS data we plot the imaginary part of the full susceptibility  $\chi$  as calculated from ARPES data as discussed above for constant  $\mathbf{q}$  cuts in Fig. 2 and constant  $\Omega$  cuts in Fig. 3. The left panels assume a constant  $U$ , the right panels the near neighbor exchange form  $U(\mathbf{q})$ . Let us first consider Fig. 2. For constant  $U$  (left panel), the resonance traces out a pronounced downwards dispersion which terminates at the node-node scattering vector  $\mathbf{q}_n$ , as seen in the INS data. For  $q < q_n$ , a distinct second branch appears, which is broad and weak, that disperses upwards. The change of behavior at  $\mathbf{q}_n$  corresponds to the so-called silent band effect and second

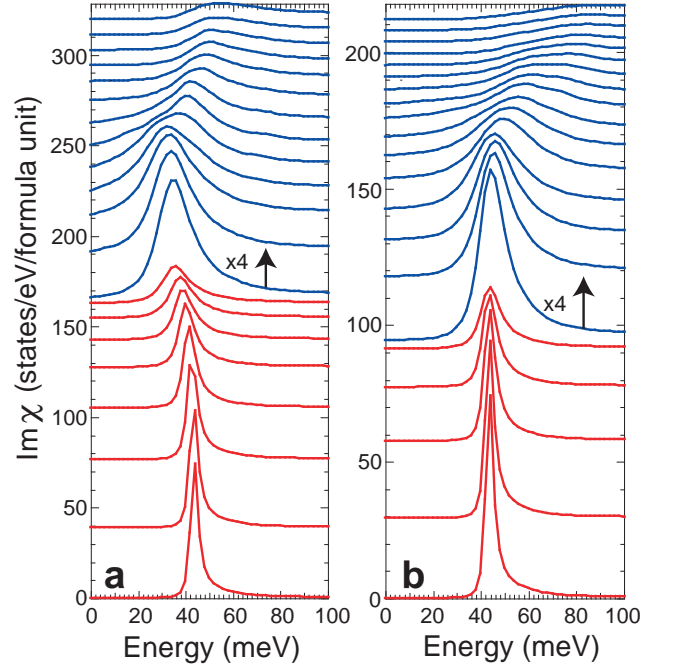


FIG. 2:  $\text{Im}\chi$  as a function of energy for several momenta  $\mathbf{q} = \eta(\pi, \pi)$  assuming (a) a constant  $U = U_0$  or (b) a near neighbor exchange  $U = U(\mathbf{q})$ . The curves, ranging from  $\eta=0.60$  (top) to  $\eta=1$  (bottom), are offset for clarity. Some curves are rescaled for visual clarity.

mode mentioned in connection with INS data of overdoped YBCO [22, 23] and Bi2212 [9]. But interestingly, the upper branch of the ‘hourglass’ is not apparent. In contrast, for  $U(\mathbf{q})$  (right panel), the mode is almost dispersionless near  $(\pi, \pi)$ , then shows an *upward* dispersion for momenta  $\mathbf{q} < 0.9(\pi, \pi)$ . This difference is a direct consequence of the relatively weak momentum dependence of  $\text{Re}\chi_0$  (Fig. 1b) coupled to the decrease in  $U(\mathbf{q})$  away from  $\mathbf{Q} = (\pi, \pi)$ .

The behavior of the dispersion observed in constant  $\mathbf{q}$  scans can be contrasted with that from constant  $\Omega$  scans (Fig. 3). For constant  $U$ , both types of scans yield a qualitatively similar mode dispersion (solid dots in Fig. 3a). However, for  $U(\mathbf{q})$ , the dispersion obtained from the constant  $\Omega$  cuts is hourglass-like, with an upward and downward branch that merge at  $(\pi, \pi)$ , in good agreement with INS data in underdoped YBCO [8]. We note that this downward branch is not visible in the constant  $\mathbf{q}$  cuts in Fig. 2b. This difference is analogous to the different ARPES dispersions that one finds from energy distribution curves as compared to momentum distribution curves.

We have also generated results involving only the GG contribution by setting  $\alpha = 0$ . In order to compare with the results having both FF and GG contribution, we rescale  $U_0$  to maintain the same resonance energy at  $\mathbf{Q}$ . Only minor differences are found between this and

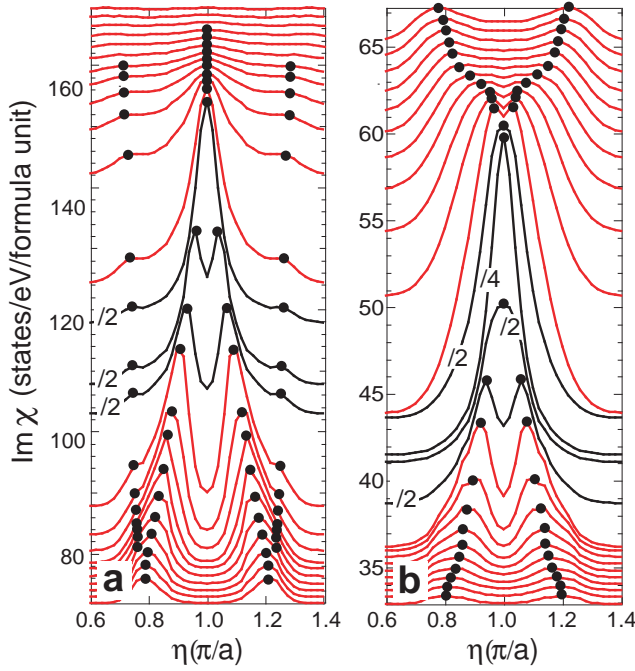


FIG. 3:  $\text{Im}\chi$  as a function of momentum  $\mathbf{q} = \eta(\pi, \pi)$  for several energies assuming (a) a constant  $U = U_0$  or (b) a near neighbor exchange  $U = U(\mathbf{q})$ . The curves, ranging from  $\Omega=68$  meV (top) to 20 meV (bottom), are offset for clarity. Some curves are rescaled for visual clarity.

the full calculation which includes both GG and FF contributions. This lack of sensitivity to the inclusion of FF terms is a consequence of the d-wave symmetry of the superconducting order parameter where  $\chi_0^G$  and  $\chi_0^F$  reinforce one another near  $(\pi, \pi)$ . (In contrast, for an s-wave superconductor,  $\chi_0^G$  and  $\chi_0^F$  are opposite in sign, and there is no spin resonance.)

Comparing our results with the INS data and earlier RPA calculations, we arrive at the following conclusions. First, the self-energy effects present in the ARPES-derived Green's function do not affect the low energy physics of spin excitations, such as the existence and sharpness of the  $(\pi, \pi)$  resonance, or the mode dispersion. Second, vertex corrections do not play a major role in the spin channel, except possibly in the overall scale of  $U$ . Third, the magnetic dispersion is sensitive to the  $\mathbf{q}$  dependence of  $U$ . Finally, our results provide strong evidence for the interpretation of the resonance peak as a spin exciton [3].

To summarize, we computed the polarization bubble  $\chi_0$  using experimental Green's functions derived from ARPES spectra, and the full dynamic spin response obtained from a diagrammatic formalism assuming either a constant or a near neighbor exchange interaction. Although this analysis requires several approximations, we find surprisingly good agreement with inelastic neutron scattering data for high temperature cuprate superconductors. Our results demonstrate a close relation be-

tween experiments probing the spin and single-particle excitations. Our formalism is quite general, and can be used as well to compute other response functions, such as the current-current response function measured by conductivity.

This work was supported by NSF DMR-0606255, NSF DMR-0513415 (D.K.M.) the U.S. DOE, Office of Science, under Contracts No. DE-AC02-06CH11357 (ANL), W-7405-Eng-82 (Ames), and Grant No. DE-FG02-05ER46225 (D.K.M.). The Synchrotron Radiation Center is supported by NSF DMR-0084402. U.C. would like to thank R. Sensarma for helpful discussions.

- 
- [1] A. Damascelli, Z. Hussain and Z.-X. Shen, *Rev. Mod. Phys.* **75**, 473 (2003); J. C. Campuzano, M. R. Norman and M. Randeria, in *The Physics of Superconductors*, Vol. 2, ed. K. H. Bennemann and J. B. Ketterson (Springer, Berlin, 2004), p. 167.
  - [2] J. Rossat-Mignod *et al.*, *Physica C* **185**, 86 (1991); H. F. Fong *et al.*, *Phys. Rev. Lett.* **75**, 316 (1995); P. Dai *et al.*, *Phys. Rev. B* **63**, 054525 (2001).
  - [3] J. Brinckmann and P. A. Lee, *Phys. Rev. Lett.* **82**, 2915 (1999); Y.-J. Kao, Q. Si and K. Levin, *Phys. Rev. B* **61**, 11898 (2000); M. R. Norman, *Phys. Rev. B* **61**, 14751 (2000) and **63**, 092509 (2001); F. Onufrieva and P. Pfeuty, *Phys. Rev. B* **65**, 054515 (2002).
  - [4] See, e.g., C.-H. Pao and N. E. Bickers, *Phys. Rev. B* **51**, 16310 (1994); E. Demler and S.-C. Zhang, *Phys. Rev. Lett.* **74**, 4126 (1995); N. Bulut and D. Scalapino, *Phys. Rev. B* **53**, 5149 (1996).
  - [5] M. Vojta and T. Ulbricht, *Phys. Rev. Lett.* **93**, 127002 (2004); G. S. Uhrig, K. P. Schmidt and M. Gruninger, *Phys. Rev. Lett.* **93**, 267003 (2004); C. D. Batista, G. Ortiz and A. V. Balatsky, *Phys. Rev. B* **64**, 172508 (2001).
  - [6] H. F. Fong *et al.*, *Nature* **398**, 588 (1999).
  - [7] M. Arai *et al.*, *Phys. Rev. Lett.* **83**, 608 (1999).
  - [8] S. M. Hayden *et al.*, *Nature* **429**, 531 (2004).
  - [9] B. Fauque *et al.*, *cond-mat/0701052*.
  - [10] A. Kaminski *et al.*, *Phys. Rev. Lett.* **86**, 1070 (2001).
  - [11] U. Chatterjee *et al.*, *Phys. Rev. Lett.* **96**, 107006 (2006).
  - [12] G. D. Mahan, *Many-Particle Physics* (Plenum, New York, 1990).
  - [13] J. R. Schrieffer, *Theory of Superconductivity* (Benjamin Cummings, Reading, MA, 1964).
  - [14] M. Randeria *et al.*, *Phys. Rev. Lett.* **74**, 4951 (1995).
  - [15] A. Kaminski *et al.*, *Phys. Rev. B* **69**, 212509 (2004).
  - [16] The background is thought to be due to surface scattering. We have checked that our final results for  $\chi$  are not qualitatively affected by its subtraction.
  - [17] ARPES data are also affected by finite energy and momentum resolutions which, in principle, can be deconvolved from the data but, in practice, have been found not to have a significant effect on  $\text{Im}G$ . See: M. R. Norman *et al.*, *Phys. Rev. B* **60**, 7585 (1999).
  - [18] See, e.g., N. Miyakawa *et al.*, *Phys. Rev. Lett.* **83**, 1018 (1999); S. H. Pan *et al.*, *Nature* **413**, 282 (2001).
  - [19] We take a finite  $\delta = 0.5$  meV for the calculation of  $\text{Re}\chi_0^G$ .
  - [20] M. R. Norman *et al.*, *Phys. Rev. B* **52**, 615 (1995).
  - [21] The resulting value of  $U_0$  is 924 meV, a reasonable num-

ber for an effective U.

- [22] S. Pailhes *et al.*, Phys. Rev. Lett. **93**, 167001 (2004).
- [23] I. Eremin *et al.*, Phys. Rev. Lett. **94**, 147001 (2005).